Appl. Phys. A 82, 639–646 (2006)
DOI: 10.1007/s00339-005-3404-0

**Applied Physics A**
**Materials Science & Processing**

P.L. TABERNA
C. PORTET
P. SIMON✉

# Electrode surface treatment and electrochemical impedance spectroscopy study on carbon/carbon supercapacitors

CIRIMAT, UMR CNRS 5085, Université Paul Sabatier, Bat 2R1, 118 route de Narbonne, 31077 Toulouse Cedex, France

**Received: 29 August 2004/Accepted: 17 August 2005**
**Published online: 22 November 2005 • © Springer-Verlag 2005**

**ABSTRACT** Power improvement in supercapacitors is mainly related to lowering the internal impedance. The real part of the impedance at a given frequency is called ESR (equivalent series resistance). Several contributions are included in the ESR: the electrolyte resistance (including the separator), the active material resistance (with both ionic and electronic parts) and the active material/current collector interface resistance. The first two contributions have been intensively described and studied by many authors. The first part of this paper is focused on the use of surface treatments as a way to decrease the active material/current collector impedance. Al current collector foils have been treated following a two-step procedure: electrochemical etching and sol-gel coating by a highly-covering, conducting carbonaceous material. It aims to increase the Al foil/active material surface contact leading to lower resistance. In a second part, carbon-carbon supercapacitor impedance is discussed in term of complex capacitance and complex power from electrochemical impedance spectroscopy data. This representation permits extraction of a relaxation time constant that provides important information on supercapacitor behaviour. The influence of carbon nanotubes addition on electrochemical performance of carbon/carbon supercapacitors has also been studied by electrochemical impedance spectroscopy.

**PACS** 82.45.Yz; 81.16.-c

## 1 Introduction

Supercapacitors are power devices used as intermediates between batteries and dielectric capacitors. Their particular performance in terms of power delivery make them suitable for applications where high power is needed over extended time periods [1, 2], i.e., from few hundred milliseconds up to around 10 s. Like conventional batteries, the maximum peak power that can be delivered by these devices is calculated from the simple (1):

$$P_{\max} = U^2/4\,\mathrm{ESR} \quad (1)$$

where $U$ is the nominal cell voltage (V) and ESR is equivalent series resistance (Ohm). Increasing the specific power requires increasing the cell voltage or decreasing the ESR. The voltage of a carbon-based supercapacitor depends mainly on three factors: (a) the electrolyte potential window stability, (b) the active material potential window stability and (c) the current collector potential window stability. The electrolyte working potential window (a) must be as high as possible and depends on the type of electrolyte used. With aqueous-based supercapacitors, it is generally limited to around 1 V, due to water electrolysis [3, 4]. When aprotic electrolytes are used, this potential window can be theoretically increased up to 3 or 4 V, limited by the redox decomposition reactions of the organic compounds [5, 6].

The active material working potential window (b) is determined by the nature of the active material used. For carbon-based active materials, the key point is the potential reached by the positive electrode during charging: it must be kept under the oxidation potential of the carbon, that appears for instance above 4.5 V/$Li^+$/Li in an acetonitrile + $NEt_4BF_4$ electrolyte. Impurities can also lead to reduction reactions during charging at the negative electrode, also limiting the cell voltage. This highlights the importance of the activated carbon purity, which must be as high as possible: redox reactions associated with the presence of impurities can decrease this working potential window.

The current collector is an important part of the supercapacitor (c). It ensures the active material polarization through its electronic conductivity. There should be no Faradic reactions associated with the current collector in a carbon-based supercapacitor. It has to be stable in the potential range explored by the positive and the negative electrode. Problems may appear at the positive electrode, where high positive potentials can be reached at the end of a constant current charge, thus leading to the degradation of the current collector by anodic oxidation. Aluminium is the most commonly used current collector in organic electrolytes, due to the passive $Al_2O_3$ layer protecting the under-lying metal [7, 8]. In aqueous electrolytes such as sulphuric acid, stainless steels can be used [9]. Nickel can be used in alkaline solutions.

These three parameters control the nominal voltage of the supercapacitor. As mentioned above, a high cell voltage is not sufficient enough to reach high power: the series resistance must be as low as possible [10]. The equivalent series resistance of a supercapacitor is the sum of various contributions, such as the electrolyte resistance, the active material

✉ E-mail: simon@chimie.ups-tlse.fr

resistance, and the active material/current collector interface resistance. The decrease of this interface resistance can be obtained by the use of surface treatment; in the first part of this paper, a surface treatment based on a sol-gel process is proposed to decrease this interface resistance.

In the second part of this paper, frequency behaviour of cells is studied by electrochemical impedance spectroscopy by using the complex model of the capacitance. Firstly, the comparison between a REC electrolytic capacitor and a carbon supercapacitor has been made to characterize the frequency behaviour of each device. Then, as the complex capacitance model can be used to characterize electrode materials, the frequency response of laboratory test cells has been studied using treated current collector. Secondly, cells using active material containing CNTs have also been characterized. Carbon nanotubes (CNTs) have been extensively studied for supercapacitor applications. Numerous papers have been focused on the use of CNTs as the active material, due to their exceptional properties [11–14]: a high electronic conductivity and a high usage efficiency of their specific surface area thanks to a unique pore texture. The frequency behaviour of cells using electrodes containing activated carbon (AC)/CNTs mixture with various compositions was studied.

## 2 Experimental

### 2.1 *Constitution of* 4 $cm^2$ *carbon/carbon supercapacitor cells*

4 $cm^2$ supercapacitors cells are assembled by laminating active material on the Al current collector foil. The active layer composition is: 95 wt. % activated carbon, 3 wt. % CMC and 2 wt. % PTFE (carboxymethylcellulose from Prolabo and polytetrafluoroethylene from Dupont de Nemours). The activated carbon used is the Picatif BP10 from the Pica Company (Vierzon, France). The active material weight is 60 mg, i.e., 15 mg/$cm^2$. The process has been described elsewhere [15].

Cell assembly is made in a high-purity argon (6.0 quality) filled glove box with both water and oxygen content lower than 1 ppm. The stack was assembled by inserting two layers of porous polymeric separators between the two electrodes. Two PTFE plates and stainless steel clamps are used in order to maintain the stack under pressure. The stack is immersed in an organic electrolyte, a solution of acetonitrile (AN, 10 ppm water) with 1.5 M $NEt_4BF_4$ dried salt.

### 2.2 *Current collector surface treatment*

Here, two types of Al current collector surface treatment are described. The first type of surface treatment is based on a sol-gel process and has been already published [16]. The etching treatment based on previous work has been developed for electrodes used in electrolytic capacitors in order to increase the surface area [17]. Here, the 4 $cm^2$ Al foils are immersed in NaOH 1 M for 20 minutes in order to degrease the foils and to generate nucleation sites for Al dissolution; then, the etching treatment is performed in 1 M HCl solution at 80 °C for 2 minutes in order to create surface roughness. In a second step, the roughened surface of the Al is coated by a conducting film via the sol-gel route, which is well-known for its high-covering power. The sol is constituted of a polymeric matrix with a conducting carbonaceous material. The polymeric matrix is prepared by condensation reactions between hexamethylenetetraamine (HMTA) and acetylacetone (Acac) in acetic acid. The sol-gel matrix permits a stable suspension of the carbonaceous particles in the sol. Carbonaceous particles have a lower size (50 nm) than the etching channels width created on the Al foil (several μm). The slurry is deposited onto the Al substrate by dip-coating with a controlled withdrawal speed in order to deposit the carbonaceous particles. A final thermal treatment is performed to decompose the polymeric matrix [16].

The second type of surface treatment consists in a vaporization of a conductive paint by a spray method. Once the Al current collectors are polished, a 20 μm thick polyurethane-based conductive paint is used; this process has been described elsewhere [15].

### 2.3 *Carbon nanotubes addition in the active material*

The active material is a mixture of AC supplied by Pica and CNTs synthesized by Arkema by a chemical vapor deposition (CVD) process: ethylene decomposition at 650 °C–700 °C on Fe-based catalyst deposited on alumina. This process leads to multiwall carbon nanotubes (MWCNTs) with an average external diameter between 10–30 nm. A chemical treatment in sulfuric acid solution is performed in order to decrease the $Al_2O_3$ and Fe content. At the same time, the ash content is decreased to 2.5 wt. %. The chemical composition is as follows: $SiO_2$ 0.02%, 0.3% $Al_2O_3$ and 1.9% $Fe_2O_3$.

The active material is obtained in the same way we described in Sect. 2.1: x wt. % of activated carbon, y wt. % CNTs ($x + y = 95\%$), 3 wt. % CMC and 2 wt. % PTFE. Several weight ratios of CNTs have been tested: 5%, 10%, 15% and 30%. Laboratory supercapacitor cells were assembled, using treated current collectors with a carbonaceous sol-gel deposit (described in Sect. 2.2).

### 2.4 *Electrochemical measurements*

Galvanostatic cycling tests were carried out with a Arbin potentiostat (BT 2000), with a sampling rate of 20 ms. Electrochemical impedance spectroscopy measurements were carried out with a Schlumberger Solartron 1255 frequency response analyzer and a Schlumberger Solartron 1286 potentiostat controlled by a computer with the software Z plot. The frequency range studied was 10 kHz–10 mHz. The $\Delta V$ applied signal amplitude was $+/-5$ mV.

## 3 Results and discussion

### 3.1 *Galvanostatic cycling tests*

The internal resistance of the supercapacitor is the sum of both electronic and ionic resistance contributions. The ionic contribution is due to the electrolyte resistance located in the separator and in the electrode porosity. The electrolyte resistance is an important part of the ESR. Aqueous electrolytes exhibit good conductivities (a few hundred mS $cm^{-1}$ for concentrated sulphuric acid solutions) but with a limited potential window (around 1 V). On the other hand,

organic electrolytes have lower conductivity (around tens of $mS\,cm^{-1}$) but lead to higher cell voltage (2.3–2.7 V) [18]. This explains why organic electrolytes are generally used in carbon-based supercapacitors: both the energy density ($E = CV^2/2$ where $C$ is the capacitance and $V$ the cell voltage) and the power density are higher as compared to aqueous electrolyte.

The active material resistance can be separated into two components: the electronic and the ionic resistances. The electronic resistance includes the intrinsic electronic conductivity of the activated carbon particles and the electronic contact between particles. These two contributions are often a minor part of the ESR: the electronic conductivity of the activated carbons can reach $1\,S\,cm^{-1}$ and some conducting agents can be added to the active material to increase the conductivity [19]. The ionic resistance is the electrolyte ionic resistance inside the pores of the electrode. It depends on the electrolyte conductivity, porous texture of the electrode and the electrode thickness [20, 21]. Thin films of active material and activated carbon with controlled porosity have reduced the influence of this contribution [22, 23].

The active material/current collector interface resistance (or impedance) shows the contact resistance between the film and the current collector. This contact resistance can be one of the major contributions, with electrolyte, to the global ESR of the supercapacitor [24]. The lack of adhesion or low surface contact between the active material film and the collector are good examples of poor interfacial impedance. In the literature, some examples of treatments are described to overcome these problems, such as conducting paint [15, 22] or mixture of CMC and acetylene black [25] coating onto the collector surface prior active material film deposit, or aluminium deposit by CVD or PVD on the active material film [26]. All these treatments are dedicated to one objective: decreasing the impedance at the active material/current collector interface.

Here, we propose another type of surface treatment based on a carbonaceous sol-gel deposit which has been described in the experimental part. Figure 1 presents the FEG-SEM (field-emission gun scanning electron microscope) picture of the Al surface after etching; it can be seen that there is a formation of channels in relation to highly controlled corrosion of the Al grains. Figure 2 presents a FEG-SEM picture of the etched Al foil covered by the carbonaceous slurry; it can be seen that the whole surface is covered by the carbonaceous particles.

Cells assembled with treated current collectors have been firstly characterized by galvanostatic cycling measurements. Figure 3 presents the cell voltage change of a $4\,cm^2$ supercapacitor cell assembled with treated Al current collectors, between 0 and 2.3 V at $+/-100\,mA/cm^2$. The linear shape of the $V = f(t)$ plot shows the absence of undesired Faradic reactions, proving that the treatment does not affect the general electrochemical characteristics of the cell. Figure 4 presents the change of the equivalent series resistance, calculated by dividing the ohmic drop measured during the current switch (from charge to discharge) by the current (here $2I$, as the same current value is used for both charge and discharge). The ESR change is given for a cell using (a) painted Al current collectors and (b) treated Al current collector as described above.

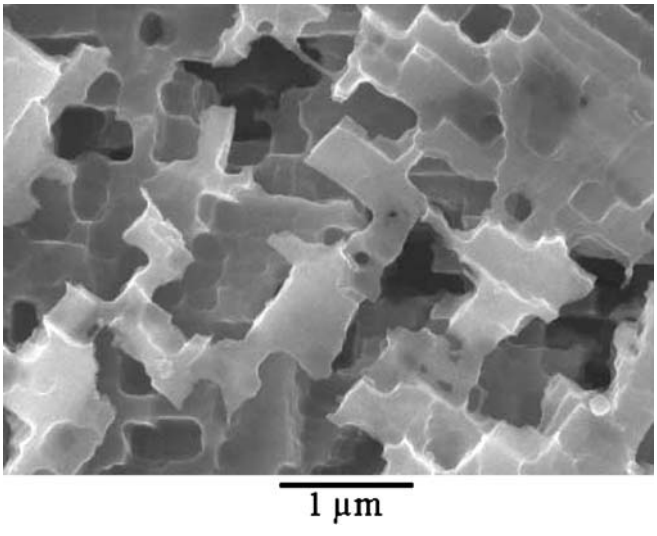


**FIGURE 1** FEG-SEM picture of an etched Al foil

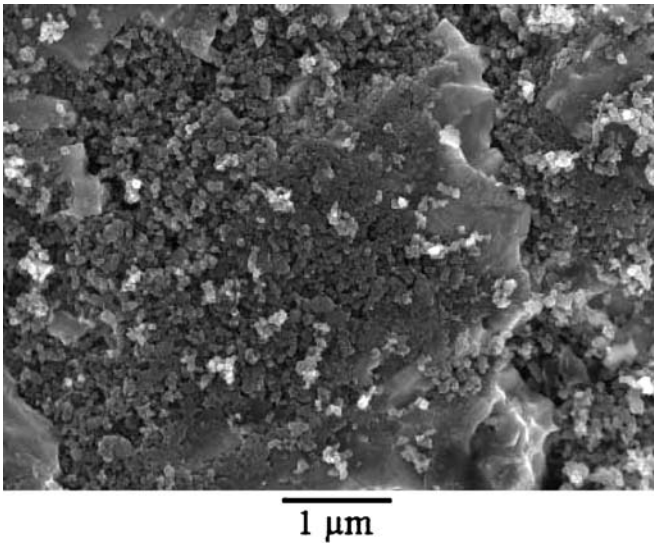


**FIGURE 2** FEG-SEM picture of an etched Al current collector, covered by a carbonaceous coating by the sol-gel route

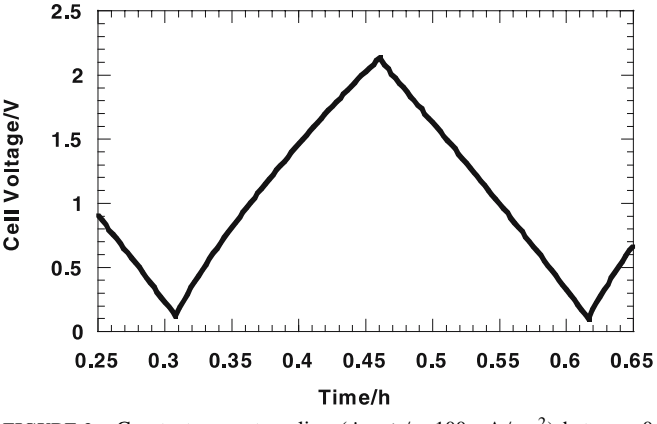


**FIGURE 3** Constant current cycling ($j = +/-100\,mA/cm^2$) between 0 and 2.3 V of a $4\,cm^2$ supercapacitor cell assembled with treated Al current collectors

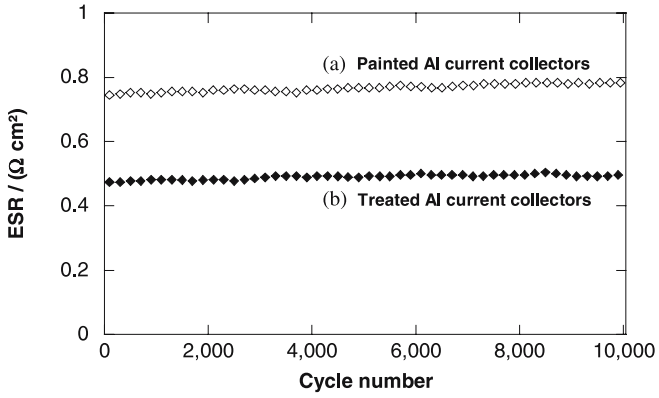


**FIGURE 4** Equivalent series resistance change during constant current cycling at $j = +/-100\,\mathrm{mA/cm^2}$ between 0 and 2.3 V for a 4 $\mathrm{cm^2}$ supercapacitor cell using (**a**) painted Al current collectors and (**b**) treated Al current collectors

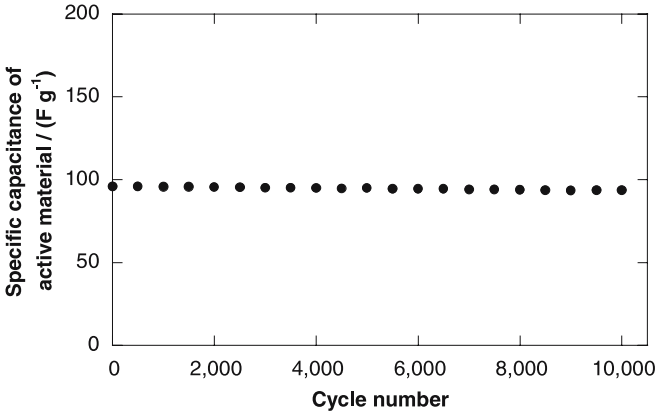


**FIGURE 5** Activated carbon specific capacitance change during the constant current cycling ($j = +/-100\,\mathrm{mA/cm^2}$ between 0 and 2.3 V) for a 4 $\mathrm{cm^2}$ supercapacitor cell using treated Al current collectors

The cell assembled with treated Al collectors has the lower specific ESR, around 0.5 $\Omega\,\mathrm{cm^2}$. This low value demonstrates the efficiency of the etching/sol-gel treatment. Both the surface and the contact between the Al current collector and the active material have been improved, since the carbonaceous sol-gel deposit covers the most important part of the etched Al surface; the ESR decrease is due to the etching and coating process since, it was shown that etched-only Al current collectors have a higher ESR [16]. The ESR is stable over the 10 000 cycles performed; the cycling test was stopped at the end of the 10 000 cycles to avoid the impact of loss of hermeticity.

During cycling, the cell capacitance is calculated from the slope of the discharge curve (Fig. 3):

$$C = \frac{I}{\left(\frac{\mathrm{d}V}{\mathrm{d}t}\right)} \tag{2}$$

where $C$ is the cell capacitance in Farads, $I$ the current in Ampere (A) and $\mathrm{d}V/\mathrm{d}t$ the slope of the discharge curve in Volt per second (V/s). Calculation is made between the maximum voltage corrected from the ohmic drop ($U_{\max} = 2.3\,\mathrm{V} - RI$, where $RI$ is the ohmic drop) down to 0 V. Figure 5 shows the specific capacitance of the activated carbon calculated according to (3):

$$C_{m_{\mathrm{AC}}} = \frac{2C}{m_{\mathrm{AC}}} \tag{3}$$

where $m_{\mathrm{AC}}$ is the active material weight (g) per electrode of activated carbon, $C_{m_{\mathrm{AC}}}$ the specific capacitance in Farad per gram of activated carbon (F/g) and $C$ the cell capacitance in Farad (F).

The specific capacitance of the activated carbon is around 95 F/g, constant over the 10 000 cycles studied; the treatment of the Al current collectors does not affect the capacitive behaviour of the cell; the same capacitance values are obtained for both cells. This carbon specific capacitance leads to a value of 90 F/g of active material, since the electrode composition is 95 wt. % activated carbon. The 4 $\mathrm{cm^2}$ cell tested exhibits improved characteristics in terms of power density ($P_{\max} = 88\,\mathrm{kW/kg}$ of active material), with a series resistance of 0.5 $\Omega\,\mathrm{cm^2}$ and a active material capacitance of 90 F/g, demonstrating the efficiency of the treatment described here. There is an increase in specific power as compared to a cell assembled with painted Al foil ($P_{\max} = 55\,\mathrm{kW/kg}$ of active material).

### 3.2 *Electrochemical impedance spectroscopy measurements*

Electrochemical impedance spectroscopy (EIS) is an helpful experimental tool to characterize frequency response of a device. The measurement proceeds by applying a low amplitude alternating voltage $\Delta V$ to a steady-state potential $V_{\mathrm{s}}$, with $\Delta V(\omega) = \Delta V_{\max} \mathrm{e}^{\mathrm{j}\omega t}$, where $\omega$ is the pulsation and $\Delta V_{\max}$ the signal amplitude. This input signal leads to a sinusoidal output current $\Delta I$, with $\Delta I(\omega) = \Delta I_{\max} \mathrm{e}^{\mathrm{j}(\omega t + \varphi)}$ where $\varphi$ is the phase angle of the current versus the voltage and $\Delta I_{\max}$ the signal amplitude. The electrochemical impedance $Z(\omega)$ is defined as $Z(\omega) = \frac{\Delta V}{\Delta I} = |Z(\omega)|\,\mathrm{e}^{-\mathrm{j}\varphi} = Z' + \mathrm{j}Z''$, where $Z'$ and $Z''$ are respectively the real part and the imaginary part of the impedance, defined as $Z'^2 + Z''^2 = |Z(\omega)|^2$.

Experimental data extracted from this measurement are usually plotted in a Nyquist diagram which represents the imaginary part of the impedance versus the real part. The well known plot is presented in Fig. 6a. Figure 6a shows the whole frequency domain while Fig. 6b is focused on a particular frequency range, between 2 kHz and the "knee frequency", where a 45 °C slope is observed. Some authors misguidedly link this part of the curve to a Warburg diffusion impedance. In fact, the driving force of the ionic adsorption in the porous electrode is the electric field applied so that the mass transport is mainly ensured by ionic migration. Thus the electrode porosity can be described by a RC network described elsewhere by a transmission line model (TLM) [27, 28]. Nyquist plots are extensively used to describe carbon-carbon supercapacitors, but do not allow easy extraction of frequency information. Complex impedance analysis is a powerful tool to describe and fit non linear electric circuits, but in our case, to describe capacitors or supercapacitors, a more suitable way is proposed by analysing frequency behaviour by complex capacitance modelling of impedance data [15]. With the help

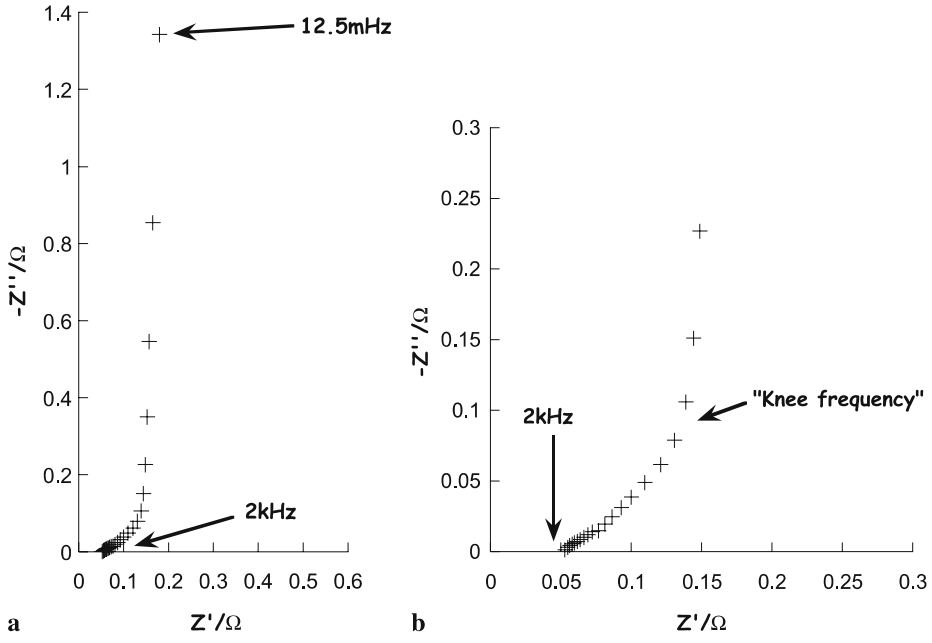


**FIGURE 6** Nyquist plot of a commercial carbon-carbon supercapacitor (2.3 V–10 F)

of (4), it is possible to define the complex capacitance as follows:

$$Z(\omega) = \frac{1}{j\omega C(\omega)} \quad \text{in ohm} \tag{4}$$

with:

$$C(\omega) = C'(\omega) - jC''(\omega) \quad \text{in Farad} \tag{5}$$

(4) and (5) lead to:

$$C'(\omega) = \frac{-Z"(\omega)}{\omega\,|Z(\omega)|^2} \quad \text{and} \tag{6}$$

$$C"(\omega) = \frac{Z'(\omega)}{\omega|Z(\omega)|^2} \tag{7}$$

both in Farad.

$C'$ represents the real part of the capacitance; it shows the variation of the available stored energy with the frequency. $C''$ represents the losses that occur during charge storage [15].

This complex model of the capacitance allows comparison of several capacitor devices as developed in the next section. Moreover, electrode materials can be validated by using this model as presented below.

*3.2.1 Comparison between aluminium electrolytic capacitor and carbon-carbon supercapacitor.* Carbon-carbon supercapacitors have larger frequency dispersion as compared to aluminium electrolytic capacitors due to the porous nature of the electrodes. Volumetric capacitances are around several Farad per cubic centimetre for carbon-carbon supercapacitors; these values are around one thousand times those obtained with aluminium electrolytic capacitors. For supercapacitors, the majority of this capacitance is only available at low frequency. Figure 7 represents the change of the real part of the capacitance $C$' with the frequency, for both devices. Dimensionless capacitance values are calculated by dividing by $C_0$, where $C_0$ is the dc capacitance: 10 F and 100 μF respectively for the supercapacitor and the electrolytic capacitor.

As seen in Fig. 7, capacitances are obtained for different frequency ranges. Full capacitance is reached below 1 kHz for the electrolytic capacitor, while no more capacitance left at frequencies higher than 1 Hz for the carbon supercapacitor.

An additional analysis can be achieved by plotting the imaginary part of complex capacitance versus frequency (Fig. 8). This graph presents the capacitive dispersion related to energy losses. The peaks observed for each device can be used to determine the typical frequency attached to the relaxation time $\tau_0$; it is a characteristic of the whole system. This relaxation time defines the limit between predominately resistive behaviour at frequencies higher than $1/\tau_0$ and capacitive behaviour at lower frequencies. This relaxation time constant is also well known as the 45° figure of merit leading to a good idea of the frequency response of the capacitor [29]. Thus,

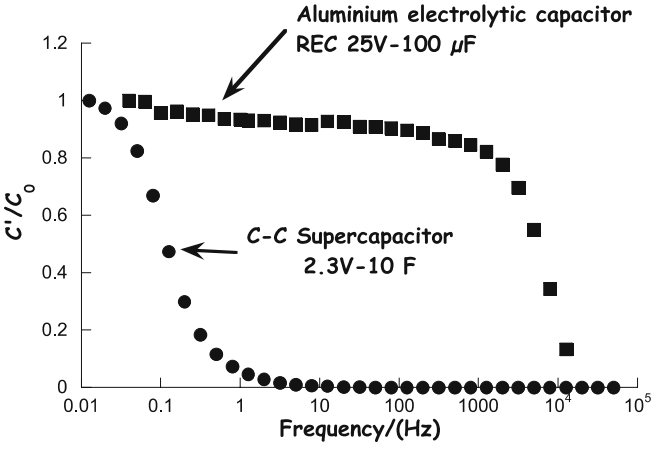


**FIGURE 7** Real part of complex capacitance vs. frequency. Comparison between a carbon supercapacitor device and a conventional aluminium electrolytic capacitor. $C_0$ is the full capacitance of the device

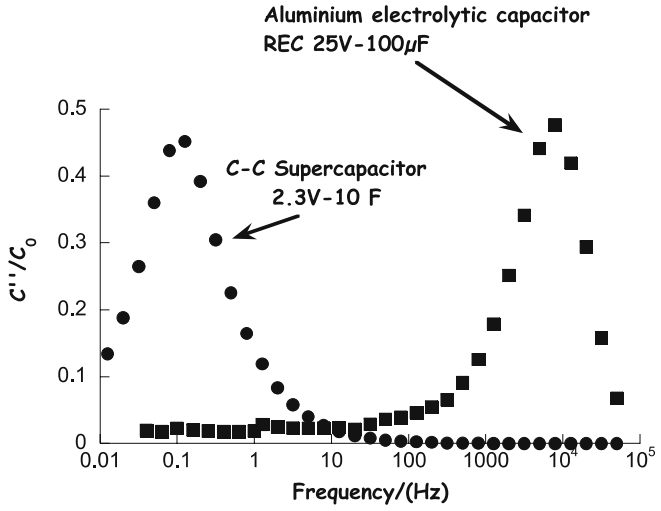


**FIGURE 8** Imaginary part of complex capacitance vs. frequency. Comparison between a carbon supercapacitor device and a conventional aluminium electrolytic capacitor. $C_0$ is the full capacitance of the device

examining the $C'$ plot, it can be noticed that half of the full capacitance is reached at $1/\tau_0$.

Relaxation time constants found for the aluminium electrolytic capacitor and carbon-carbon supercapacitor are respectively 126 μs and 7.94 s. It confirms an expected result that electrolytic capacitors are better designed for high power over short periods than supercapacitors storing 1000 times more energy density. Whatever the type of capacitor, the complex capacitance model from impedance data is an easy way to point out the relaxation time constant of a system and get its optimal frequency domain. Moreover, it can indicate the power improvement that can be deduced from this relation time constant [15].

To go further, complex capacitance can also be helpful to select suitable electrode active materials, surface treatments or electrolytes. The next section deals with the influence of both surface treatment on the current collector and addition of carbon nanotubes on frequency behaviour of the carbon-carbon supercapacitor.

*3.2.2 Surface treatment influence on supercapacitor frequency behaviour.* In Sect. 3.1 of this paper, it has been demonstrated that power improvement (ESR decrease) of supercapacitors using a treated current collector is mainly linked to good contact between the current collector and active material. A sol-gel route has been appropriate to achieve a surface contact improvement at this interface and a large decrease in ESR is obtained. This section focuses on frequency response of supercapacitor cells using such a carbonaceous interlayer. The comparison is made between a sprayed conductive paint and the etched/sol-gel coating. Both of these surface treatments have been described in the first part of this paper.

Figure 9a presents the real part of the capacitance ($C'$) for the two types of surface treatment and Fig. 9b, the imaginary part ($C''$). Both the surface treated current collectors have the same real and imaginary maximal capacitance values: 2 F and 0.45 F for respectively $C'$ and $C''$. As observed before, contact impedance between active material and current collector directly affects the equivalent series resistance. Thus, the main effect is a frequency response enlargement when coating the current collector via sol-gel route because of higher covering power as compared to spray conductive paint, so that a lower relaxation time constant is obtained: 7.93 s for sol-gel route versus 12.6 s for conductive paint. It means that the energy can be stored and delivered faster for a supercapacitor using treated current collectors. The carbonaceous layer coating via sol-gel route improves the supercapacitor power.

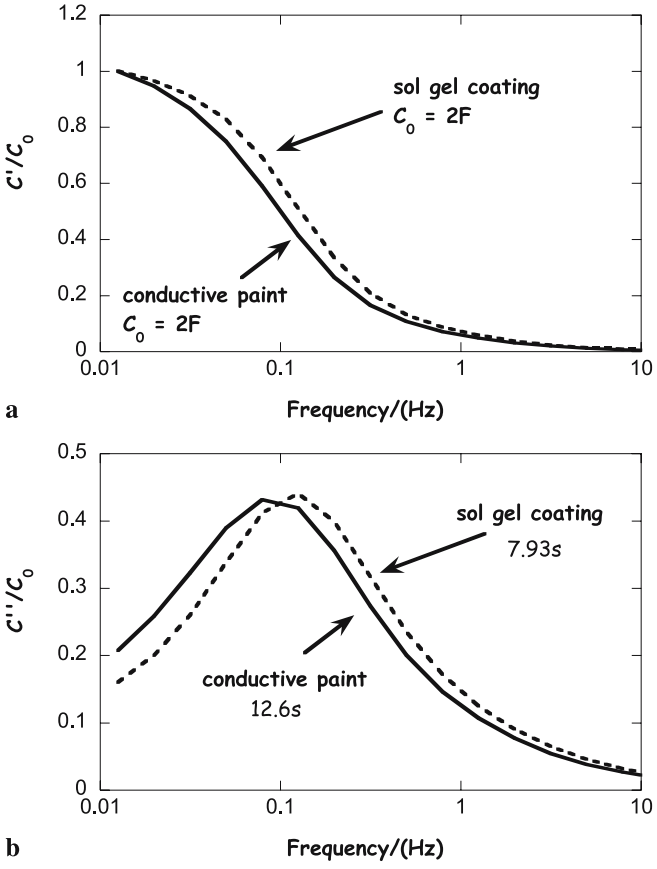


**FIGURE 9** Evolution of the real part (**a**) and imaginary part (**b**) of capacitance vs. frequency for 2.3 V–2 F supercapacitor laboratory cell

### 3.3 *Influence of carbon nanotubes on supercapacitor frequency behaviour*

Figure 10a and b present $C'$ and $C''$ plots for several weight ratios of carbon nanotubes in activated carbon. Regarding real capacitance $C'$, there is an expected ongoing slight decrease when the CNT content is raised. As compared to 0% weight content, the capacitance diminutions are respectively for 5 wt. %, 10 wt. %, 15 wt. % and 30 wt. %: 4.5%, 4.5%, 9% and 14%. This decrease in capacitance is due to the lower capacitance of CNTs which is estimated at around 50 F/g versus 100 F/g for Picactif activated carbon. CNT addition may be expected to cause linear decrease capacitance, but this is not the case; capacitance loss is moderated by another effect: enhancement of both ionic and electronic percolation networks resulting from CNT presence in the active material; CNTs form an open mesoporous network which makes easier the ion adsorption and limits the cap-

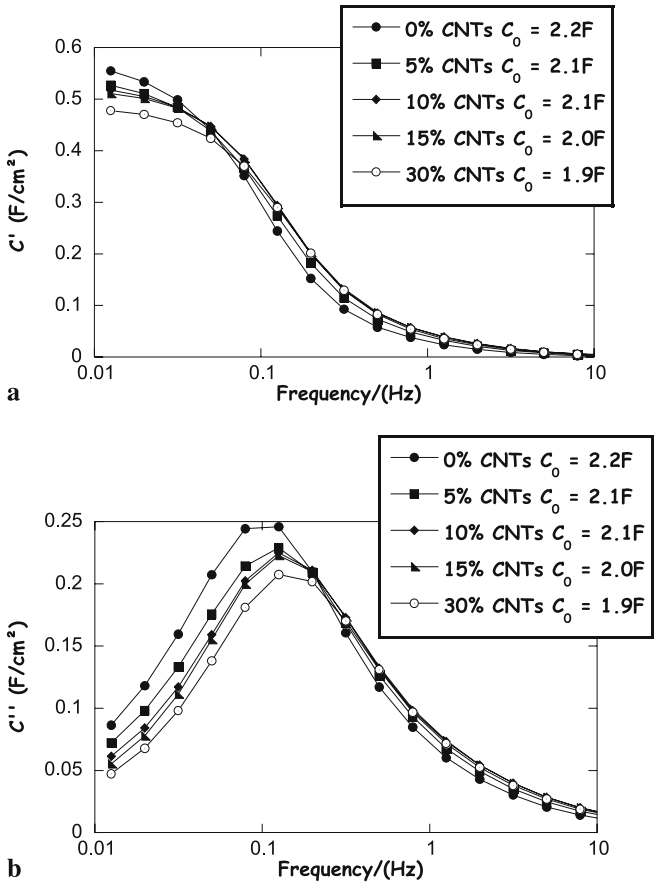


**FIGURE 10** Performance of 4 $cm^2$ supercapacitor cells assembled with treated Al current collectors and CNTs/activated carbon mixture with different compositions. Evolution of the real part (**a**) and imaginary part (**b**) of the capacitance vs. frequency

acitance loss when CNT content increases in the active material [30, 31]. As described by the transmission line model for porous electrodes: the lower the ohmic drop, the higher the capacitance [31, 32]. Figure 10b shows that the frequency peak is shifted toward higher frequencies when CNTs content increases.

From Fig. 10b, the relaxation time constant is deduced. Figure 11 plots the variation of this relaxation time constant with CNT content. It can be seen that the relaxation time constant decreases with increasing content of CNT. For a value of 15% of CNTs, $\tau_0$ exhibits a large decrease as compared to a cell using electrodes containing only activated carbon. For 30% CNT content, the relaxation time constant only very slightly further decreases. A cell assembled with electrodes containing CNTs will deliver higher power density with a relatively small loss of capacitance. This is shown in the cell resistance values listed in Table 1. When the CNT content is increased, the ESR decreases but a sharp decrease is observed for 15% CNTs. For such a content, both electronic and ionic conductivities are improved.

| CNTs (wt. %) | 0 | 5 | 10 | 15 | 30 |
|---|---|---|---|---|---|
| $ESR_{1\,kHz}$ ($\Omega\,cm^2$) | 0.5 | 0.48 | 0.45 | 0.4 | 0.39 |

**TABLE 1** ESR values measured at 1 kHz extracted from Nyquist plots for different CNTs content in the active material

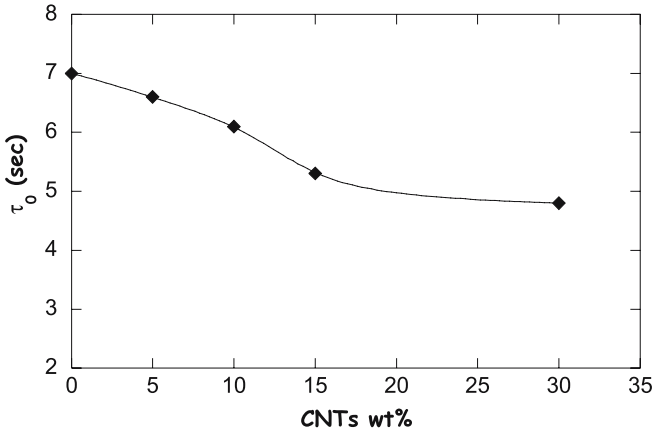


**FIGURE 11** Variation of relaxation time constant with CNTs content

Thus, 15% of CNTs appears to be a good compromise between stored energy and delivered power; the ESR and the relaxation time constant show a major decrease and the capacitance loss is limited as compared to a cell using activated carbon based electrodes.

The complex capacitance model clearly highlights capacitance as a function of frequency; permitting easy determination of the usable frequency range to obtain optimal power and energy from of the device.

## 4 Conclusion

The first part of this paper presents a surface treatment of the Al current collector based on a sol-gel deposit which aims to decrease the Al/active material interface resistance. The comparison between supercapacitor cells assembled with treated current collectors and painted current collectors in organic electrolyte has been presented. A lower ESR is obtained for a cell using sol-gel treated current collectors as compared to a cell using painted current collectors, leading to a higher delivered power where capacitance is equivalent for both cells.

The second part of this paper focuses on the frequency behaviour study of cells by using the complex model of the capacitance; this model allows observation of the variation of the capacitance with the frequency and deduction of the relaxation time constant. An aluminium electrolytic capacitor and a carbon-carbon supercapacitor have been compared. A larger frequency range is obtained for the electrolytic capacitor where the capacitive behaviour appears at higher frequency leading to a very low relaxation time constant as compared to supercapacitor.

This model shows that the frequency response of cells using treated Al current collectors exhibits a lower relaxation time constant than that obtained with cells using painted current collectors. These treated cells are able to deliver their stored energy faster.

Various compositions of activated carbon/CNT mixtures in the active material have been studied. With increasing CNT content, the ESR and the relaxation time constant decrease, associated with a reduced capacitance loss at higher frequency. A value of 15% of CNTs is a good compromise be-

tween delivered power (low ESR and $\tau_0$) and stored energy (high capacitance).

## REFERENCES


1 A. Burke, J. Power Source **91**, 37 (2000)
2 S. Nomoto, H. Nakata, K. Yoshioka, A. Yoshida, H. Yoneda, J. Power Source **97–98**, 807 (2001)
3 M.S. Ding, K. Xu, J.P. Zheng, T.R. Jow, J. Power Sources **138**, 340 (2004)
4 M. Ue, In: Proc. of the 8th International Seminar on Double-Layer Capacitors and Similar Energy Storage Devices, Deerfield Beach, FL, December 7–9, 1998
5 B.E. Conway, *Electrochemical Capacitor: Scientific: Fundamentals and Technological Applications* (Plenum, New York 1999), p. 105
6 R. Kötz, M. Carlen, Electrochim. Acta **45**, 2483 (2000)
7 B.W. Ricketts, C. Ton-That, J. Power Source **89**, 64 (2000)
8 E. Lust, A. Jänes, M. Arulepp, J. Electroanal. Chem. **562**, 33 (2004)
9 C-T. Hsieh, H. Teng, Carbon **40**, 667 (2002)
10 S. Yoon, J. Lee, T. Hyeon, S.M. Oh, J. Electrochem. Soc. **147**, 2507 (2000)
11 C. Emmenegger, P. Mauron, P. Sudan, P. Wenger, V. Hermann, R. Gallay, A. Züttel, J. Power Source **124**, 321 (2003)
12 Q. Xio, X. Zhou, Electrochim. Acta **48**, 575 (2003)
13 E. Frackowiak, S. Delpeux, K. Jurewicz, K. Szostak, D. Cazorla-Amoros, F. Béguin, Chem. Phys. Lett. **361**, 35 (2002)
14 A.K. Chatterjee, M. Sharon, R. Nanerjee, M. Neumann-Spallart, Electrochim. Acta **48**, 3439 (2003)
15 P.L. Taberna, P. Simon, J.F. Fauvarque, J. Electrochem. Soc. **148**, A292 (2003)
16 C. Portet, P.L. Taberna, P. Simon, C. Laberty-Robert, Electrochim. Acta **49**, 905 (2004)
17 R.S. Alwitt, H. Uchi, T.R. Beck, R.C. Alkire, J. Electrochem. Soc. **131**, 13 (1984)
18 M. Ue, M. Takeda, M. Takehara, S. Mori, J. Electrochem. Soc. **144**, 2684 (1994)
19 M.S. Mickael, S.R.S. Prabaharan, J. Power Source **136**, 250 (2004)
20 G. Salitra, A. Saffer, L. Eliad, Y. Cohen, D. Aurbach, J. Electrochem. Soc. **147**, 2486 (2000)
21 Y.J. Kim, Y. Horie, S. Ozaki, Y. Matsuzawa, H. Suezaki, C. Kim, N. Miyashita, M. Endo, Carbon **42**, 1497 (2004)
22 A. Du Pasquier, J.A. Shelburne, I. Plitz, F. Badway, A.S. Gozdz, G.G. Amatucci, In: Proc. of the 11th International Seminar on Double-Layer Capacitors and Similar Energy Storage Devices, Deerfield Beach, FL, December 3–5 (2001)
23 A. Celzard, F. Collas, J.F. Marêché, G. Furdin, I. Rey, J. Power Source **108**, 153 (2002)
24 J.P. Zheng, J. Power Source **137**, 158 (2004)
25 K. Nakao, K. Shimizu, T. Yamaguchi, European Patent Application, Matsushita Electric, EP 0 948 005 A1 (1999)
26 A. Nishino, U.S. Patent, Matsushita, 4 621 607 (1985)
27 R. de Levie, Electrochim. Acta **8**, 751 (1963)
28 R. de Levie, Electrochim. Acta **9**, 1231 (1964)
29 J.R. Miller, In: Proc. of the 8th International Seminar on Double-Layer Capacitors and Similar Energy Storage Devices, Deerfield Beach, FL, December 7–9 (1998)
30 C. Portet, P.L. Taberna, P. Simon, E. Flahaut, J. Power Source **139**, 371 (2004)
31 F. Pico, J.M. Rojo, M.L. Sanjuan, A. Anson, A.M. Benito, M.A. Callejas, W.K. Maser, M.T. Martinez, J. Electrochem. Soc. **151**, A831 (2004)
32 R. Kötz, M. Carlen, Electrochim. Acta **45**, 2483 (2000)